2014-01-01

Characterization Of Membrane Interaction Of Mycobacterium Tuberculosis ESAT-6

Yue Ma
University of Texas at El Paso, my8335@gmail.com

CHARACTERIZATION OF MEMBRANE INTERACTION OF *MYCOBACTERIUM TUBERCULOSIS* ESAT-6

YUE MA

Department of Biological Sciences

APPROVED:

Jianjun Sun, Ph.D., Chair

Jianying Zhang, Ph.D

Chuan Xiao, Ph.D.

Hugues Ouellet, Ph.D

Bess Sirmon-Taylor, Ph.D.
Interim Dean of the Graduate School

DEDICATION

To my husband, mother and father
-Thank you for all of your support

CHARACTERIZATION OF MEMBRANE INTERACTION OF *MYCOBACTERIUM TUBERCULOSIS* ESAT-6

by

YUE MA, Ms

THESIS

Presented to the Faculty of the Graduate School of

The University of Texas at El Paso

in Partial Fulfillment

of the Requirements

for the Degree of

MASTER OF SCIENCE

Department of Biological Sciences

THE UNIVERSITY OF TEXAS AT EL PASO

May 2014

ACKNOWLEDGEMENTS

I want to thank my mentor Dr. Jianjun Sun for his teachings and advice to progress in my career. The knowledge I have gained in his laboratory has given me the opportunity to appreciate the field of bacteriology and biochemistry. I also want to thank my Committee Members Dr. Jianying Zhang, Dr. Hugues Ouellet and Dr. Chuan Xiao for their advice in my research. Learning from their perspective in the sciences allowed me to gain a better appreciation of the importance of being open to different points of view in research. I also want to thank my lab mates from whom I learned a lot not only about their perspective in science but their cultures as well due to the diversity in our lab, and thank my friend Ningjing Lei, who gave me a lot of support both in school and my personal life. I want to thank my mom and my dad for all of their support and encouragement to push myself to try new experiences and expand my knowledge in different fields of science. I also want to thank my husband for all of his support throughout these years.

ABSTRACT

Mycobacterium tuberculosis (Mtb) targets alveolar macrophages and has a high tolerance to the macrophage's antimicrobial effectors, such as low pH, reactive oxygen species, and reactive nitrogen species. It has been reported and widely accepted that Mtb disarms macrophages through arresting the normal maturation process of the phagosomes. Inhibition of phagosome-lysosome fusion and phagosome acidification is an effective survival strategy at the early stage of infection. This behavior allows Mtb to remain and replicate within the phagosomes of macrophages. At the later stage of infection, the pathogen translocates from the phagolysosomal compartments into the cytosol of host cells by phagolysosomal rupture. The main protein involved in virulence is known as MtbESAT-6, which is secreted by the ESX-1 secretion system and reportedly shows membrane-lysing properties. The ESX-1 secreting system is essential for the toxicity of MTB. The membrane interacting activity of MtbESAT-6 plays an important role during the infection. In this study, N- and C-terminal truncations and Cysteine mutations on the protein were generated to determine the role of N- and C-terminal flexible loops of MtbESAT-6 in membrane-interaction and the key membrane-interacting residues of MtbESAT-6. A series of fluorescence assays, including ANS, ANTS/DPX and Tryptophan, have demonstrated that both N- and C- terminal flexible loops were crucial for the membrane-interacting activity, suggesting a model that the loop area of the protein initiate the membrane attachment and the central helix-turn-helix inserts into the membranes. The study of ESX-1 secreting system, especially the molecular mechanism of MtbESAT-6 membrane interaction, is essential for us to understand how this virulence factor contributes to bacterial infection, and eventually

will facilitate development of novel therapeutics against tuberculosis.

TABLE OF CONTENTS

LIST OF FIGURES

CHAPTER 1: INTRODUCTION

1.1 *MYCOBACTERIUM TUBERCULOSIS* AND THE DISEASE

Mycobacterium tuberculosis (Mtb) is an aerobic, non-motile bacillus, which grows within cells of a host organism, and can be cultured in the laboratory setting. The bacteria divides every 16 to 20 hours and has a well-developed unique cell wall that contains a considerable amount of many fatty acids including mycolic acid, providing an extraordinary lipid barrier giving it the unique property of acid-fast staining for identification. This unique barrier is responsible for many of the medically challenging physiological characteristics of Mtb, including resistance to antibiotics and host defense mechanisms. Mtb infection begins when the mycobacteria reach the pulmonary alveoli, where they invade and replicate within endosomes of alveolar macrophages. Reportedly, approximate 10% lifetime chance that the latent infection will progress to active tuberculosis disease. Tuberculosis of the lungs may also occur via infection from the blood stream. This hematogenous transmission can also spread infection to more distant sites, such as peripheral lymph nodes, the kidneys, the brain, and the bones. According to the 2011 annual report by the World Health Organization (WHO) [1, 2], 8.7 million people fell ill with tuberculosis (TB) and 1.4 million died. In the same year, a total of 10,521 new TB cases were reported in the United States, an incidence of 3.4 cases per 100,000 population, which is 6.4% lower than the rate in 2010 (Fig. 1.1).

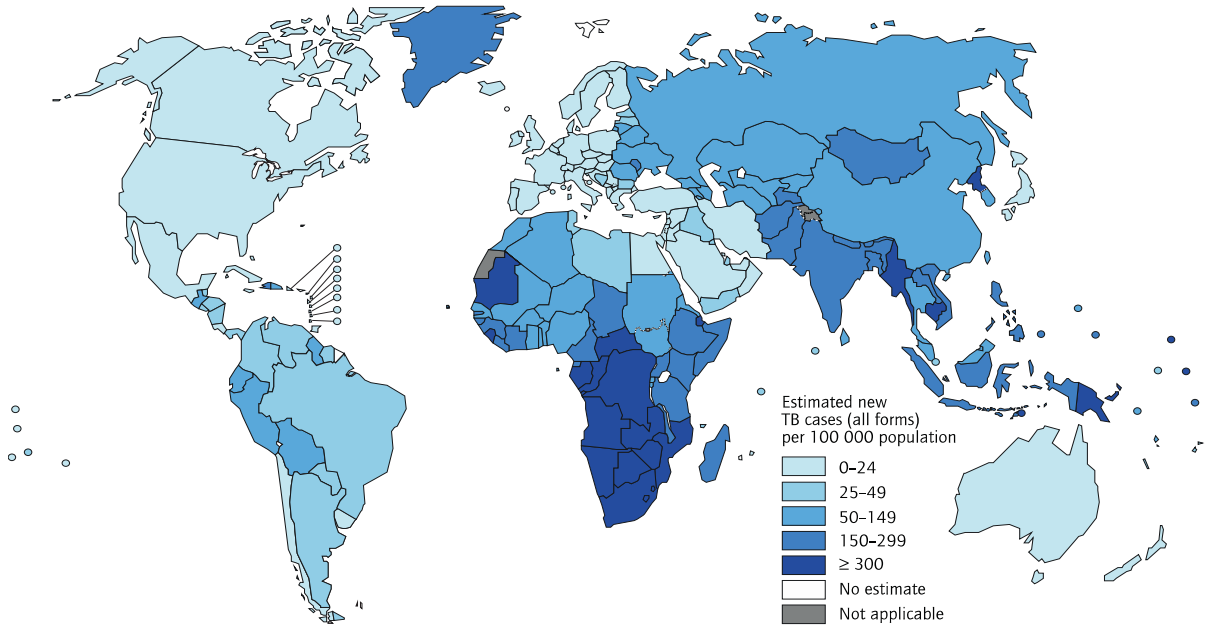

Figure 1.1: WHO report of tuberculosis cases during 2011 worldwide. (http://www.whadvocacy.com/node/255,WHO)

1.2 BCG

The bacilli Calmette-Guerin (BCG) vaccine, discovered in 1921 by Albert Calmette and Camille Guerin, is used to prevent tuberculosis with an efficacy of 80% [3]. BCG is a live avirulent bovine tuberculosis bacillus (*Mycobacterium bovis*). Because the living bacilli evolve to make the best use of the available nutrients, they become more adapted to their traditional environment, human blood, and no longer induce the disease when introduced into a human host for their preservation. Immunogenic activity however is still retained due to their wild type ancestry similarity.

This attenuated strain failed to escape from the macrophage due to the lack of a 6kD early secretory antigenic target protein (ESAT-6, EsxA, or Rv3875) and its 10kD culture

filtrate protein partner (CFP-10, EsxB, or Rv3874) due to the deletion of the region of difference 1 (RD1) [4].

1.3 RD1

RD1 is considered to be the primary attenuating deletion in the related BCG vaccine strain (Fig. 1.2). The genes of the RD1 region encode a secretory apparatus, termed ESX-1, which is responsible for exporting CFP-10 and ESAT-6, as a heterodimer [5]. It has been reported that the products of Rv3870 and Rv3871 may work together to form a membrane-bound ATPase [6]. The function of two super families of repetitive proteins Rv3872 (PE) and Rv3873 (PPE) are still unknown. Rv3876 encodes a protein with a proline-rich N-terminal region and homology in its C-terminal portion to a *Pseudomonas aeruginosa* protein involved in flagellar biosynthesis, including a deviant Walker A [6]. Rv3877 is an integral membrane protein of unknown function. The last ORFs in RD1 (Rv3878 and 3879c) are reported not essential for Mtb virulence as they are interrupted in at least one virulent clinical Mtb [6].

ESAT-6 and CFP-10 have become of great interest in recent years due to their membrane interacting activity. However, the mechanism is not well understood. Evidences are needed to confirm all reported functions of ESAT-6 and CPF-10.

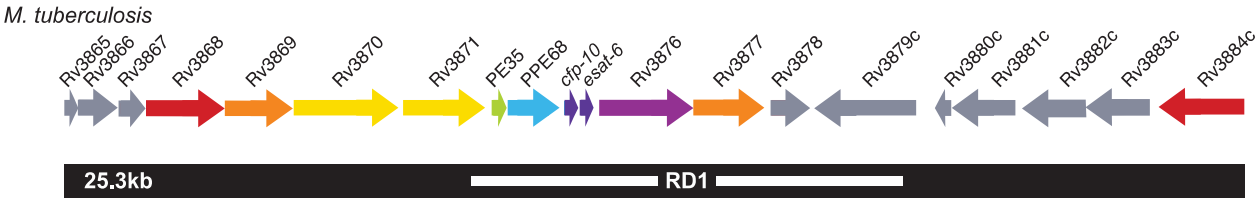

Figure 1.2: The genes in RD1 region of Mtb. [7]

1.4 ESAT-6/CFP-10

The esx-1 locus comprises of 11 genes that encode the ESX-1 secretion system and two secreted proteins: MtbESAT-6 and MtbCFP-10. ESAT-6 and CFP-10 are secreted in pair by ESX-1. Biochemical analysis has shown that MtbESAT-6 and MtbCFP-10 form a 1:1 heterodimeric complex [8, 9, 10] (Fig. 1.3).

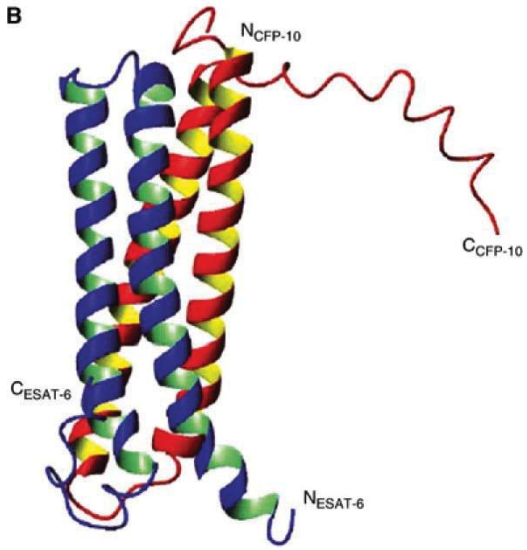

Figure 1.3: ESAT-6/CFP-10 heterodimer. [11]

1.5 SURVIVAL OF MTB IN PHAGOSOME

Mtb, but not BCG, has diverse strategies for evading host immune system. Normally, - after bacteria are engulfed into phagosomes by macrophage, phagosomes fuse with lysosomes and mature into the phagolysosomes. Phagolysosome undergoes an acidification, and bacteria are killed at this stage by the acidic condition and the hydrolases inside of the phagolysosome [9, 11]. BCG undergoes the same process as described above, but for Mtb, at the latent phase, it prevents fusion of phagosomes and lysosomes. Inhibition of phagosome-lysosome fusion is attributed to limited entrance of

lysosomal hydrolases to Mtb and inhibited acidification of phagosomes [12, 13] At the reactivation phase of Mtb infection, the phagosome-lysosome fusion occurs and MtbESAT-6 and MtbCFP-10 disrupt the membrane and translocates to the cytosol (Fig. 1.4) [14, 15].

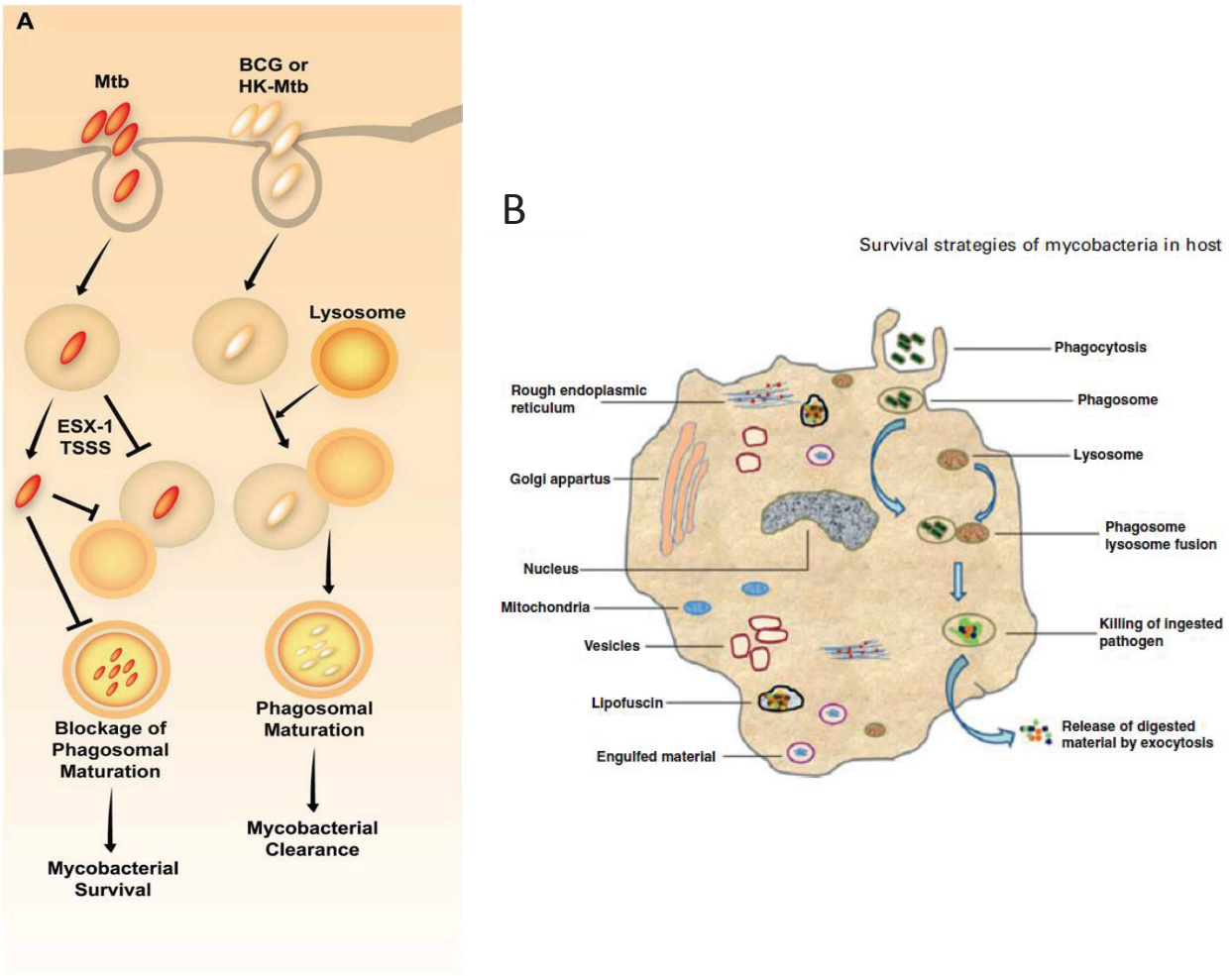

Figure 1.4: A. A schematic diagram of Mtb infection and clearance via the autophagic pathway. [16]

1.6 FUNCTION OF MTBESAT-6

MtbESAT-6 has been documented to have three important functions in virulence. It blocks maturation of phagosome where the bacteria are located. It also aids in prevention of fusion of the phagosome to lysosome so that the digestive enzymes in the lysosome can't damage the bacteria. It has also been widely documented that MtbESAT-6 allows bacteria to escape into the cytosol for replication [17, 18]. However, the specific mechanisms are still unknown. More evidence is needed to gain insight into the roles of MtbESAT-6 in Mtb pathogenesis [19, 20, 21].

1.7 SPECIFIC AIMS

Specific Aim 1:

Hypothesis: ESAT-6 proteins from Mtb and from *Mycobacterium smegmatis*, a non-pathogenic mycobacterium, have different membrane-interacting activities.

Aim: Express and purify ESAT-6 and CFP-10 from *Mycobacterium smegmatis*, which is a collaborative project comparing membrane interaction of MtbESAT-6 and MsESAT-6

Specific Aim 2:

Hypothesis: The N- and C-terminal flexible loops of ESAT-6 initiate the membrane attachment in membrane interaction.

Aim: Determine the role of N- and C-terminal flexible loops of ESAT-6 in membrane interaction using N- and/or C-terminal truncation mutants.

Specific Aim 3:

Hypothesis: The helix structures of ESAT-6 protein insert into the lipid membrane to form a pore.

Aim: Map the membrane-insertion residues of ESAT-6 using NBD fluorescence

Specific Aim 4:

Hypothesis: The ESAT-6 pores on the membranes have a discrete size.

Aim: Determine the size of ESAT-6 pores using PEGs with different molecular weights.

CHAPTER 2: MATERIALS AND METHODS

2.1 EXPRESSION AND PURIFICATION OF MSCFP-10 AND MSESAT-6

MsESAT-6 gene was amplified by PCR and cloned onto the vector pET22b between *Nde* I and *Xho* I restriction sites to produce a C-terminally His-tagged protein. MsCFP-10 gene was amplified by PCR and cloned into the vector pGEX4T *BamH* I/*EcoR* I sites to produce a N-terminally GST-tagged protein. The constructs pET22b-MsESAT-6 and pGEX4T-MsCFP-10 were transformed into *Escherichia coli* BL21 (DE3) cells, and grew overnight on LB plate, and the cells were grown at 37°C in 1 liter of LB medium containing 100 µg/ml carbenicillin in the incubator. 1 mM of IPTG (final concentration) was added to induce protein expression at OD_{600} = 0.6-1.0. Induction lasted 3 hours at 37°C for pET22b-MsESAT-6, and 6 hours at 30°C for pGEX4T-MsCFP-10. The cells were harvested by centrifugation (11,000 rpm, 15 min). Then the cells expressing MsESAT-6 protein (Insoluble, use on-column refolding) were lysed by sonication in the wash buffer (50 mM TrisHCl, 10 mM EDTA, 0.5% Triton X-100, pH 8.0). Inclusion bodies were collected by centrifuging at 15,000 rpm for 15 min at 4 °C. The resulting pellet (inclusion bodies containing ESAT-6 proteins) was washed three times with the wash buffer. The pellet was suspended and incubated in the denaturing buffer (8 M urea, 1 mM EDTA and 100 µM PMSF, pH 7.4) for 3 h at room temperature, followed by centrifugation at 17,000 rpm for 1 h at 10 °C. At the same time, Ni^{2+} -charged sepharose column was equilibrated with the equilibration buffer (20 mM Tris-Cl, 8 M urea, and 20% glycerol, pH 7.4). The supernatant was loaded onto the equilibrated column after centrifugation. Additional 300 ml of equilibration buffer was run through the column in order to wash off unbound proteins. The bound proteins were refolded on the column by

gradually removing urea with a 0-88% linear gradient of refolding buffer (20 mM Tris-Cl, 500 mM NaCl, 20% glycerol, pH 7.4) on an ÄKTA FPLC (GE Healthcare) at a flow rate of 0.5 ml/min overnight. The refolded proteins were then eluted from the column with a 0-100% linear gradient of the elution buffer (20 mM Tris-Cl, 500 mM NaCl, 20% glycerol, 250 mM imidazole, pH 7.4) at a flow rate 4 ml/min. The fractions then were collected from the FPLC, followed by SDS-PAGE to identify the proteins. All the fractions containing the target proteins were pooled, concentrated and applied to gel filtration chromatography using a Superdex-75 column in the buffer (20 mM TrisHCl, 100 mM NaCl, pH 7.4). Finally, the purity of the proteins was examined in SDS-PAGE and the proteins were stored at -80°C in small aliquots [22].

For GST-MsCFP-10 protein (soluble, purify from the supernatant), cells were re-suspended by Buffer A (PBS, pH 7.3) containing lysozyme with gentle stirring at 4°C for 30 min. Subsequently, the cells were lysed by sonication in the buffer A. The supernatant was obtained by centrifuging the lysate at 15,000 rpm for 1 hour at 4 °C. The supernatant was loaded onto the pre-equilibrated glutathione Sepharose 4B column (GS4B). The unbound proteins were washed off the column with 300 ml of buffer A. The bound proteins were eluted with a 0-100% linear gradient of Buffer B (50 mM TrisHCl, 10 mM reduced glutathione, pH 8.0) on an ÄKTA FPLC (GE Healthcare) at a flow rate of 5 ml/min. The eluted fractions were collected and examined by SDS-PAGE to identify the proteins. The fractions containing GST-MsCFP-10 were pooled. For thrombin digestion, the purified GST-CFP-10 proteins were incubated with thrombin (1 unit/100 µg of protein) at room temperature for 14 h. The thrombin-treated samples were then passed through a GS4B column. The GST and the un-cleaved GST-MsCFP-

10 were bound to the column, while the cleaved CFP-10 was collected in the flow through fractions. The resulting cleaved CFP-10 is at least 90% pure.

2.2 Purification of MsESAT-6/MsCFP-10 Heterodimers

The purified His-tagged MsESAT-6 proteins were incubated with 3 times in molar ratio of the purified MsCFP-10 in the binding buffer (20 mM Tris-Cl, 100 mM NaCl, pH 7.3) at room temperature for 2 hours. The mixture was loaded into a pre-equilibrated Ni^{2+}-column, on which the His-tagged protein complexes bound. The column was washed three times with the binding buffer to wash off free MsCFP-10 proteins, and the bound proteins were eluted with a linear gradient of the elution buffer (20 mM Tris-Cl, 100 mM NaCl, 500 mM imidazole, pH 7.3). The eluted proteins were applied to gel filtration using the Superdex 75 column, and the fractions of the heterodimer was then collected, concentrated to at least 1 mg/ml and stored at -80 °C [22].

2.3 Native Gel Shift Assay

1 μM of MsCFP-10 was incubated with MsESAT-6 at various concentrations (0.5, 1.5, and 2 μM, respectively) at room temperature (RT) for 2 h. The samples were applied to native gel electrophoresis, followed by Coomassie Brilliant Blue staining [22].

2.4 Liposome Preparation

1, 2-dioleoyl-sn-glycero-3- phosphocholine (DOPC) (20 mg/ml in chloroform) was dried under nitrogen gas to form a lipid film, followed by vacuum overnight to remove residual solvent. The dry lipid film was rehydrated by six freeze-thaw cycles in 10 mM HEPES (pH 7.4) and 150 mM KCl, and then extruded by passage through a 200-nm pore size polycarbonate filter in a mini-extruder. The liposome solution was applied to a G-25

desalting column equilibrated with 10 mM HEPES (pH 7.4) and 150 mM NaCl for buffer exchange [22, 23, 24].

2.5 K^+ Release Assay

200 µl of the K^+-doped liposomes were added into 5 ml of 10 mM buffers at various pH (sodium acetate (NaAc), pH 5.0; HEPES, pH 7.0) containing 150 mM NaCl. The purified proteins were injected into the solution with continuous stirring (final concentration 3 µM). Release of K^+ from liposomes was monitored using a K^+-selective electrode (Orion Research) connected to a microcomputer pH/mV/Temp meter 6171. The signal was transmitted by a data transmitter (DATAQ) and displayed with DATAQ software [22, 23, 24].

2.6 Expression and Purification MtbESAT-6, truncations P1, P2, and P3

The gene of N-terminal amino acids 1-10 deletion (P1), C-terminal amino acids 85-95 deletion (P2) and both N- and C- terminal deletion (P3) were obtained by PCR (Fig. 2.1). Gene P1 and P3 were cloned on to the vector pGEX4T separately to produce GST-tag proteins. Gene P2 was cloned onto vector pET22b to produce His-tag proteins. Protein P1 and P3 were expressed and purified the same way as MsCFP-10 as described above. And protein P2 was expressed and purified with the same way as MtbESAT-6 protein as described above.

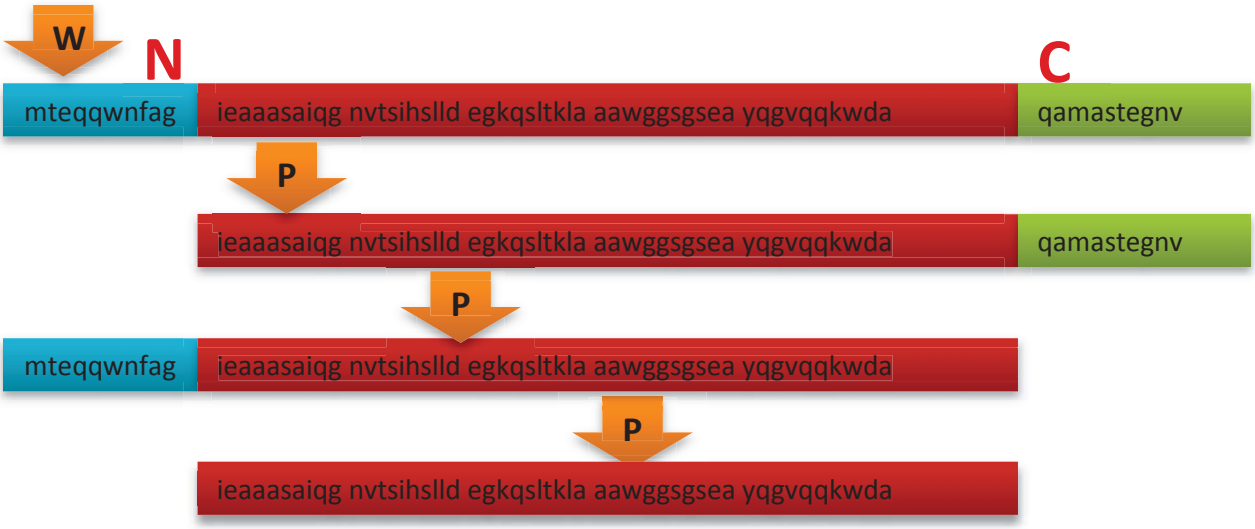

Figure 2.1: P1: N-terminal amino acids 1~10 deletion. P2: C-terminal amino acids 85~95 deletion. P3: both N- and C- terminal deletion.

2.7 The Time-Lapse Intensity Measurement of ANTS/DPX Dequenching

The liposomes containing the dye/quencher pair, 8-aminonapthalene-1, 3, 6-trisulfonic acid (ANTS)/p-xylene-bispyridinium bromide (DPX), were prepared by the same way as K^+ release (described above, desalting buffer: 5 mM HEPES, 150 mM NaCl, pH 7.3). Rehydrating solution: 50 mM ANTS, 50 mM DPX, 5 mM HEPES (pH 7.3).

The ANTS fluorescence dequenching was measured in an ISS-K2 multiphase frequency and modulation fluorometer (excitation: 380 nm, emission: 520 nm). 100 μg of purified P1, P2, P3 and WT MtbESAT-6 (Control) were separately diluted into regular gel filtration buffer (20 mM Tris-Cl, 100 mM NaCl, pH 7.3 final volume 1.3 ml) that contains 100 μl of the prepared liposomes and incubated at RT for 30 min. The solution then was loaded into cuvette with continuous stirring. After the baseline was stabilized, 200 μl of low pH buffer (50 mM NaAc, 150 mM NaCl, pH 4.0) was injected into the cuvette, and the fluorescence signal was monitored in real time. Crossed polarizers on

excitation and emission beams, and a 395-nm long-path filter were used to reduce the background scatter (Fig. 2.2) [22].

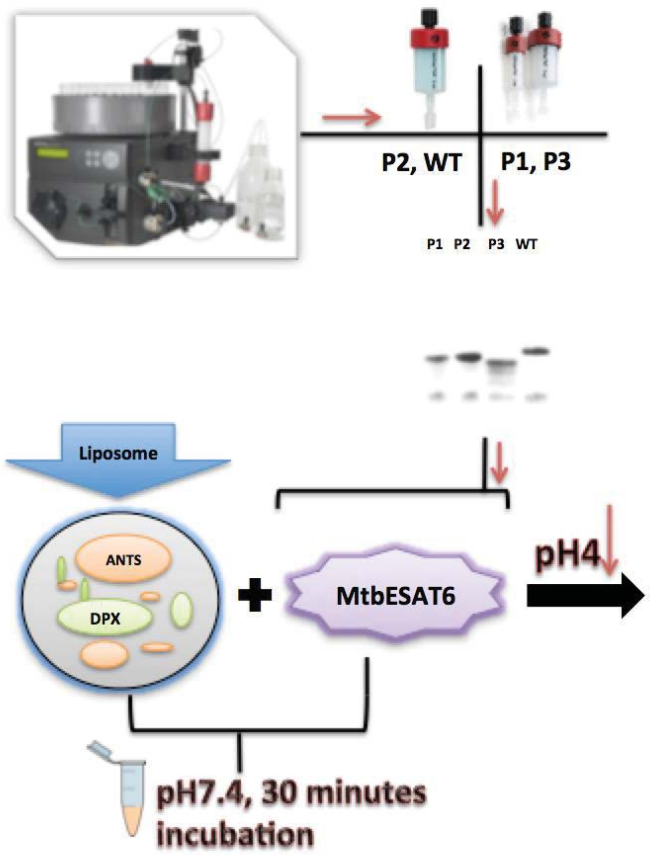

Figure 2.2: ANTS/DPX fluorescent assay

2.8 ULTRAVIOLET CIRCULAR DICHROISM (CD)

20 µM of P1, P2 and P3 were prepared separately in 10 mM pH 5.0 and pH 7.0 NaH_2PO4/Na_2HPO_4 buffer. Samples were scanned at wavelengths between 180 and 260 nm in a CD spectropolarimeter.

2.9 Intrinsic Tryptophan Fluorescence

10 μM of the purified proteins (P1, P2, P3 and WT MtbESAT-6 as control) were incubated either in a neutral pH buffer (20 mM TrisHCl, 100 mM NaCl, pH 7.0) or an acidic buffer (20 mM NaAc, 100 mM NaCl, pH 4.0) for 30 min. The intrinsic tryptophan fluorescence was measured in the ISS-K2 fluorometer (excitation: 295 nm, emission: 310–450 nm). A 305 nm long-path filter was applied in the emission channel to reduce the background. The emission spectra of the proteins were calibrated with the emission spectra of the same pH buffers without proteins in VINCI software.

2.10 ANS Fluorescence

5 μM of MtbESAT-6 or MsESAT-6 were incubated with 100 μM of 8-anilino-1-naphthalenesulfonate (ANS) in either pH 7.0 or pH 5.0 buffers for 30 min at dark. The ANS emission spectra of the samples were measured in the ISS-K2 fluorometer with excitation at 380 nm and emission at 400–600 nm. A 395 nm long-path filter was placed in the emission path to reduce the backgrounds. The emission spectra of the samples were calibrated with the same buffers (pH 7.0 or pH 5.0) without proteins in VINCI software (Fig. 2.3) [22].

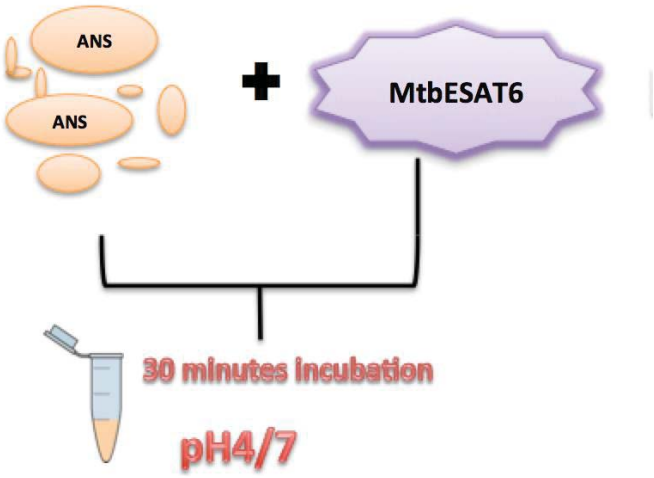

Figure 2.3: ANS fluorescent assay

2.11 CYS SUBSTITUTION MUTANTS CONSTRCTION

4th, 10th, 34th, 37th, 45th, 55th, 60th, and 88th residues were chosen to produce Cys substitution mutants. “Quickchange” mutation methods were used to obtain Cys substitution MtbESAT-6 mutants. Protein purification protocol was the same as “ on-column” refolding as described above.

2.12 THE NBD FLUORESCENCE ASSAY

IANBD [N, N’-dimethyl-N- (iodoacetyl)-N’- (7-nitrobenz-2-oxa-1, 3-diazol) ethylenediamine] was added at a 10-fold molar excess of the proteins in the presence of 10mM of reducing agent TCEP, and the mixture was incubated for over night at 4 °C (At dark). Next day, the free dye was removed by size exclusion chromatography HiPrep 26/10 desalting column. Fractions of the NBD-labeled protein were pooled together and stored at –80 °C. The labeling efficiency was estimated by absorbance spectrophotometry (ε_{478} = 25,000 M^{-1} cm^{-1} for NBD, and ε_{280} = 17990 M^{-1} cm^{-1} for

MtbESAT-6). The liposomes were prepared with regular gel filtration buffer (Fig. 2.4) [22].

The NBD fluorescence was measured in an ISS-K2 multiphase frequency and modulation fluorometer (excitation: 488 nm, emission: 544 nm). 200 μg of labeled proteins Q4C, G10C, Q34C, T37C, G45C, Q55C, A60C, and G88C were separately diluted into regular gel filtration buffer that contains 100 μl of the prepared liposomes. Incubate at RT for 30 min at dark. The solution then was loaded into cuvette with continuous stirring. After the base line was stabilized, 200 μl of low pH buffer (50 mM NaAc, 150 mM NaCl, pH 4.0) was injected into the cuvette, and the fluorescence signal was monitored in real-time. Crossed polarizers on excitation and emission beams, and a 515 nm long-path filter were used to reduce the background scatter.

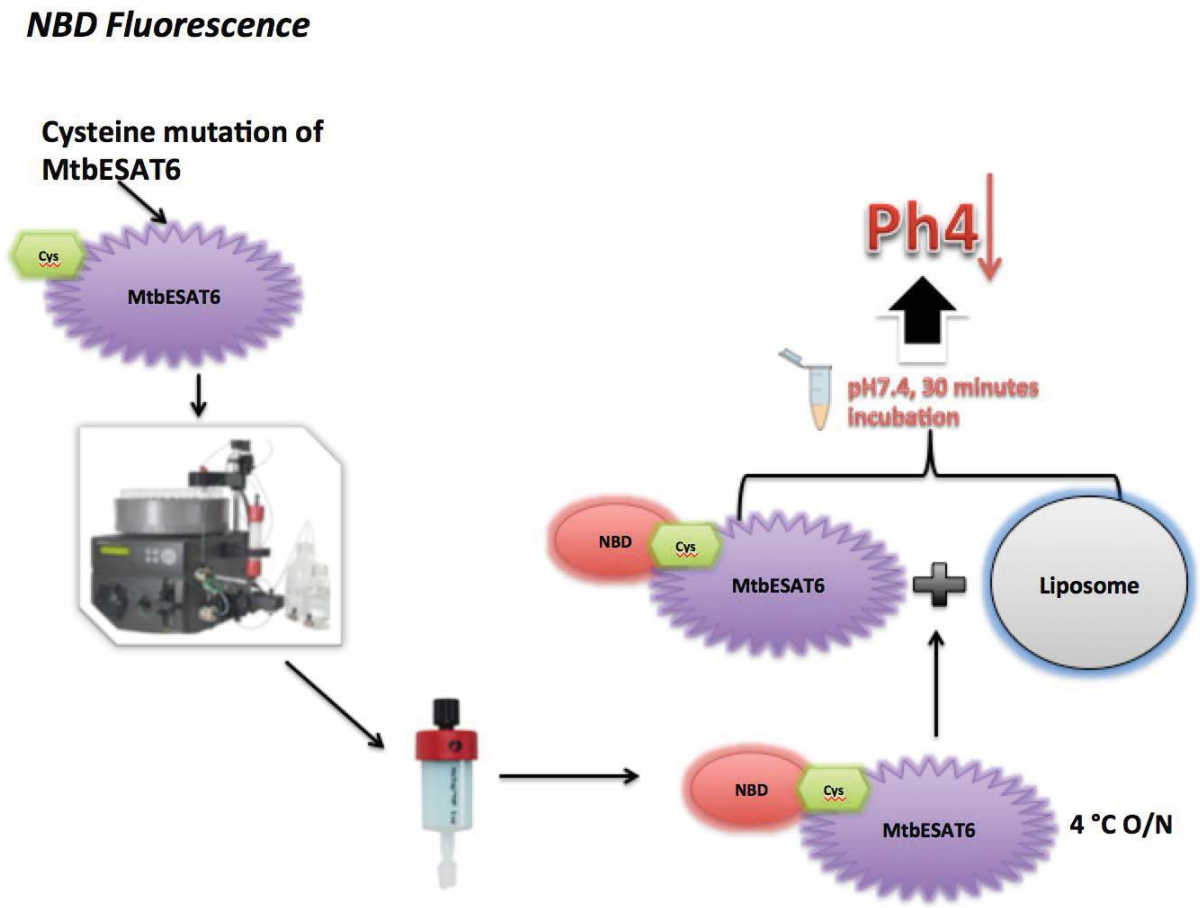

Figure 2.4: NBD fluorescent assay

2.13 PEGS PREPARITION AND ANTS/DPX DEQUENCHING ASSAY

PEG600, 1000, 2000, 2500, 3000, 4000, 6000, 8000 were prepared as 50mM stock concentration then stock at -20 °C. The protocol followed the previously described ANTS/DPX dequenching assay except one more step was added: 5 mM of PEGs were added separately into the gel filtration butter that contains 100 µg of WT MtbESAT-6 protein and 100 µl of liposomes and incubated for 30 min (Fig. 2.5).

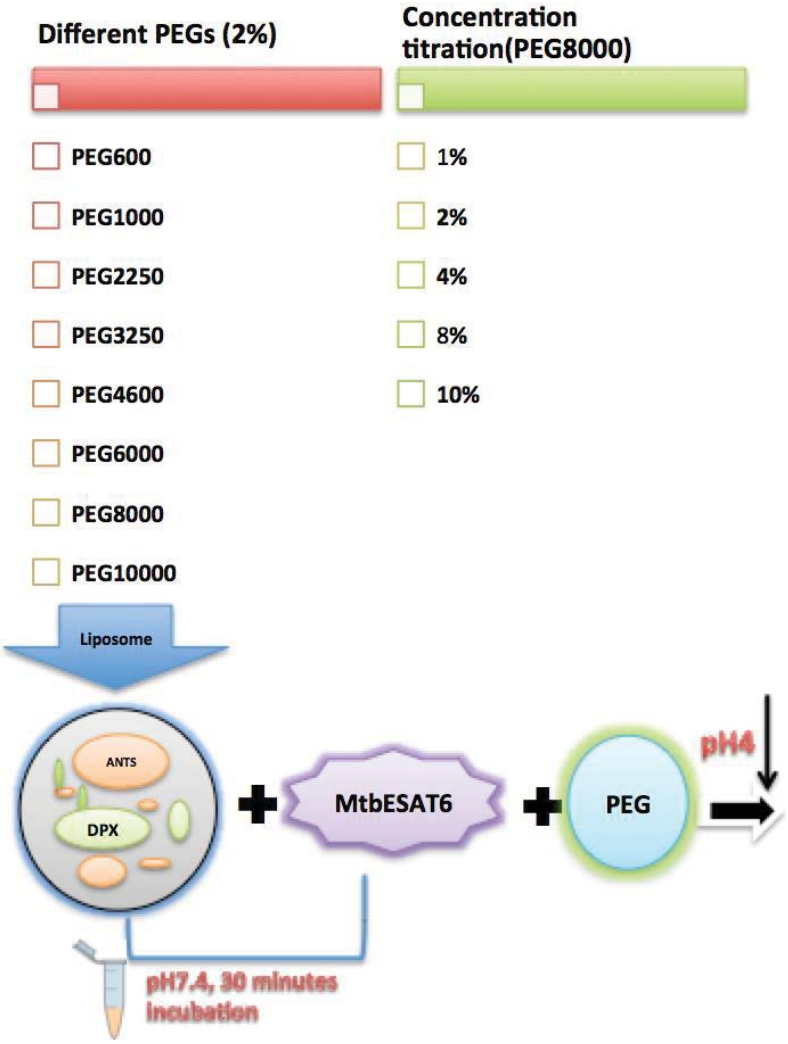

Figure 2.5: ANTS/DPX fluorescent assay with PEGs

CHAPTER 3: RESULTS

3.1 EXPRESSION AND PURIFICATION OF MSCFP-10 AND MSESAT-6

On-column refolding and purification protocol was used to minimize protein degradation and increase the purification efficiency. The purified MsESAT-6 protein is soluble in aqueous solution and migrates as a single band in SDS-PAGE with at least 90% purity. MsCFP-10 was expressed soluble and was purified with GST tag protocol. After thrombin treatment, the cleaved MtbCFP-10 was purified as a soluble protein with above 90% purity (Fig. 3.1B).

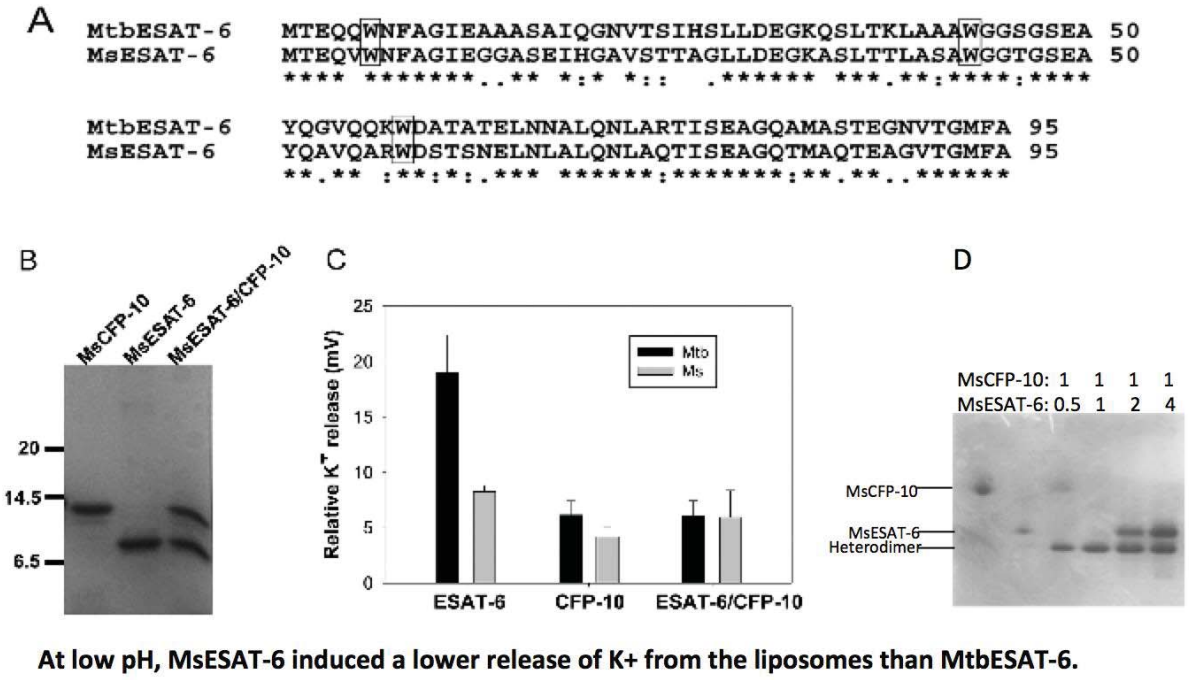

Figure 3.1: A. Sequence alignment of MtbESAT-6 and MsESAT-6. **B**. Recombinant proteins of MsESAT-6, MsCFP-10, and MsESAT-6/ CFP-10 heterodimer were purified and examined by SDS-PAGE, followed by Coomassie staining. **C**. 3 μM of the indicated proteins were injected into the liposome solutions at pH 5.0. The release of K^+ ions from the liposomes at 60 s of post-injection was measured and quantified from at least three independent experiments. **D.** Native gel shift binding assay. MsESAT-6 and MsCFP-10 were incubated at the indicated molar ratio at pH 7.0 and then applied to native gel electrophoresis, followed by Coomassie Blue staining.

3.2 NATIVE GEL SHIFT BINDING ASSAY OF MSESAT-6/MSCFP-10 SHOWS 1:1 BINDING

The purified MsESAT-6 and MsCFP-10 bound to each other in a dose-dependent manner, and formed a heterocomplex that migrated as a distinct band as indicated in the native gel electrophoresis (Fig. 3.1D).

3.3 Compared with MtbESAT-6, MsESAT-6 Induced Little Release of K^+ from the Liposomes

MsESAT-6 shares high sequence homology with MtbESAT-6, including most of the conserved hydrophobic residues (Fig. 3.1*A*). MtbESAT-6, MtbCFP-10, and the MtbESAT-6/CFP-10 heterodimer were purified by a colleague. K^+ release assay then was carried out. At low pH, the level of K^+ release induced by MsESAT-6 was significantly lower than that induced by equal amount of MtbESAT-6. MsCFP-10 and the MsESAT-6/CFP-10 heterodimer induced little release of K^+ as their Mtb-counterparts (Fig. 3.1*C*)

3.4 At low pH, P1, P2 and P3 induced a weaker leakage of the membrane vesicles containing ANTS/DPX than wild type MtbESAT-6

ANTS/DPX, the anion/cation fluorophore/quencher pair, is widely used for membrane leakage measurement [25, 26]). ANTS fluorescence is quenched by DPX when they are close together inside the liposomes, and it is dequenched upon release into the solution. As expected, addition of WT MtbESAT-6 caused significant membrane lysis and induced a sharp increase of ANTS fluorescence, while P1, P2 and P3 proteins induced much lower fluorescence dequenching, especially for P3.

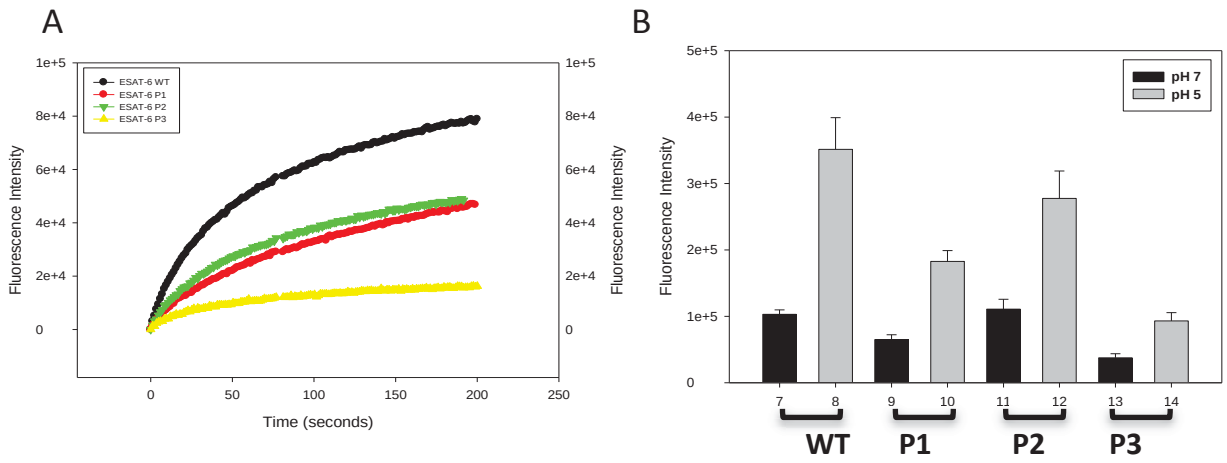

Figure 3.2: At low pH, P1, P2 and P3 induced a weaker leakage of the membrane vesicles containing ANTS/DPX than wild type MtbESAT-6. Liposomes containing the dye/quencher pair, ANTS/DPX, and the proteins (100 µg per reaction) were diluted into a pH 7.4 buffer with continuous stirring. Once the fluorescence base line was stabilized, 200 µl pH 4.0 buffer was injected into the solution. The dequenching of ANTS fluorescence due to leakage of the membrane vesicles was recorded at emission 520 nm with excitation at 380 nm. The representative recordings of ANTS dequenching are shown in **A**. The fluorescence intensity at 200 s of post-injection was quantified from three independent measurements and shown in **B**.

3.5 P1, P2 AND P3 WERE FOLDED CORRECTLY AT PH 5.0 AND PH 7.0

Ultraviolet circular dichroism (CD) measures the secondary and tertiary structure of proteins. Measurements can be made on proteins in the solution phase, and critically time-resolved measurements can be made with millisecond resolution. This approach has been widely used for investigating protein folding. Spectra for all proteins WT MtbESAT-6, P1, P2 and P3 all showed stronger folding at low pH, especially for P1 and P3 [27].

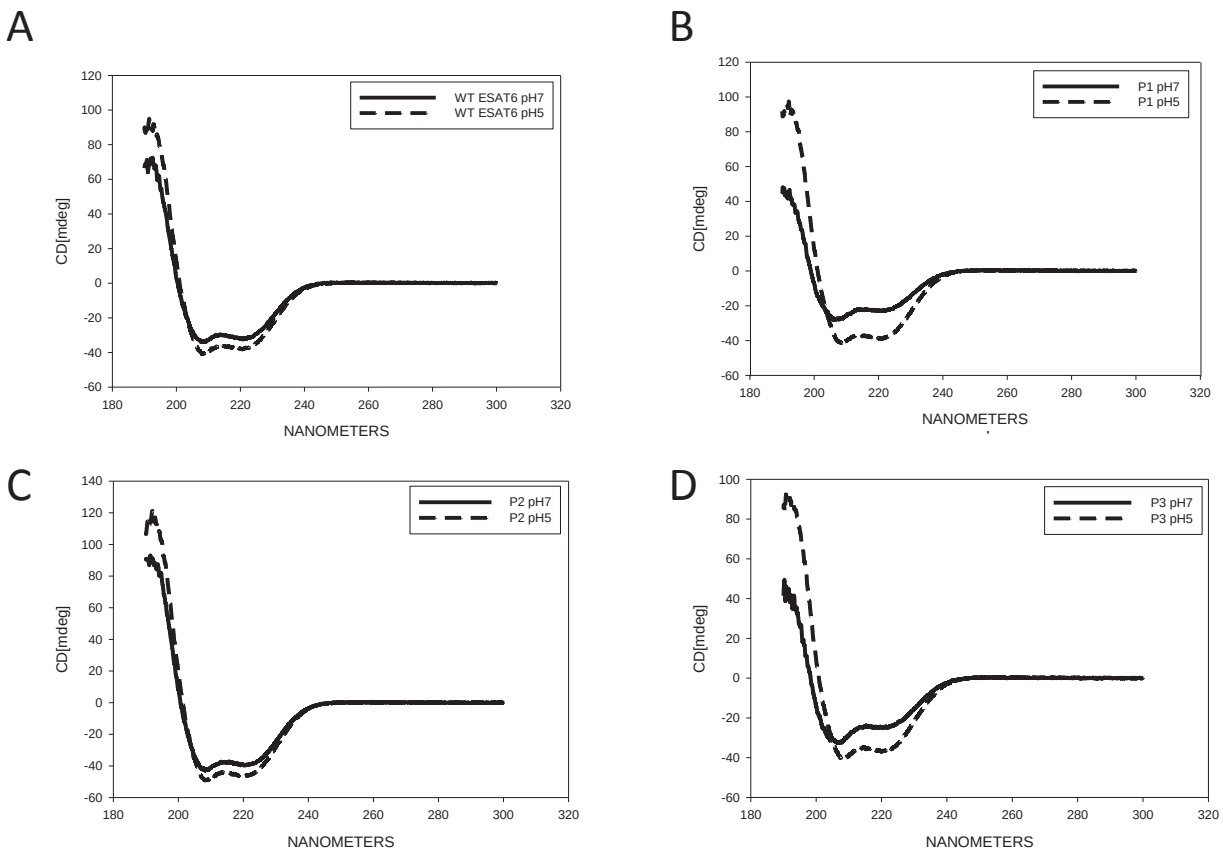

Figure 3.3: Wavelengths from 190 nm to 300 nm were scanned and plotted in **A**. WT MtbESAT-6; **B**. P1; **C**. P2; **D**. P3. The spectra in the far UV region between 180 and 260 nm, which reported secondary structure, suggested proteins folded correctly and even tighter at pH 5.0 for all four proteins, especially on P1 and P3. Predicted secondary structure percentages (http://k2d3.ogic.ca/): WT pH 7.0: α helix: 81.52%, β strand: 0.31%; WT pH 5.0: α helix: 94.1%, β strand: 0.26%; P1 pH 7.0: α helix: 68.16%, β strand: 0.41%; P1 pH 5.0: α helix: 94.44%, β strand: 0.27%; P2 pH 7.0: α helix: 93.99%, β strand: 0.27%; P2 pH 5.0: α helix: 94.58%, β strand: 0.3%; P3 pH 7.0: α helix: 68.08%, β strand: 0.39%; P3 pH 5.0: α helix: 93.62%, β strand: 0.27%.

3.6 At low pH, membrane interactions of wild type, P1, P2, and P3 were associated with a reduced solvent-exposed hydrophobicity. P1, P2 and P3 exhibited weaker ANS fluorescence upon acidification.

To further confirm that the pH-dependent membrane interaction is due to an increased solvent-exposed hydrophobicity, an extrinsic fluorescence dye, 8-anilino-1-naphthalenesulfonate (ANS), was used to measure change of hydrophobic residues after acidification. ANS was incubated with the proteins either at pH 5.0 or pH 7.0 (Fig. 3.4). ANS is hardly fluorescent in aqueous environment, but becomes highly fluorescent when it binds to hydrophobic sites of proteins. As expected, P1, P2 and P3 showed little ANS fluorescence at both pH 7.0 and pH 5.0, comparing with MtbESAT-6, suggesting that P1, P2 and P3 have less solvent-exposed hydrophobic residues at neutral pH, and its conformation is less responsive to acidification, especially for P3.

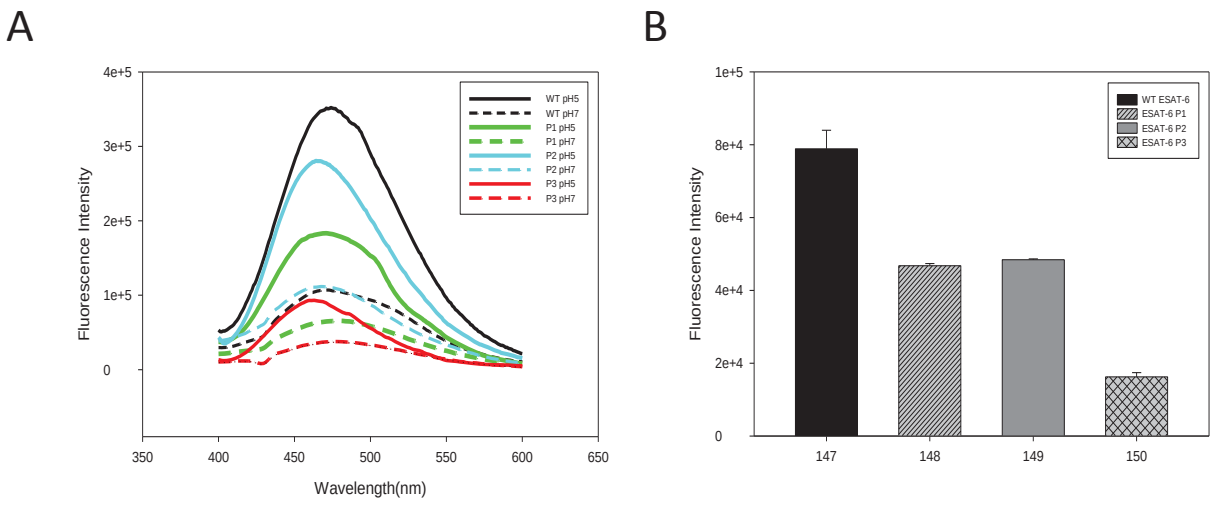

Figure 3.4 At low pH, membrane interactions of wild type, P1, P2 and P3 were associated with a reduced solvent-exposed hydrophobicity. P1, P2 and P3 exhibited weaker ANS fluorescence upon acidification. 5 μm MtbESAT-6 WT, P1, P2 or P3 were incubated with 100 μm of ANS at either pH 7.0 or pH 5.0 buffers for 30 min. The samples were excited at 380 nm and the emission fluorescence intensity of ANS was recorded at 400–600 nm. The emission spectra of the samples were calibrated with the same buffers (pH 7.0 or pH 5.0) without proteins. The representative results are shown in **A**. The difference of peak emission intensity at 468 nm (pH 5.0 and pH 7.0) was quantified from at least three independent experiments and shown in **B**.

3.7 ACIDIFICATION TRIGGERED A STRONGER CONFORMATIONAL CHANGE ON P1, P2 AND P3 THAN WT MTBESAT-6.

Transition of an aqueous-soluble protein into a membrane-interacting protein is always accompanied by significant conformational changes. Therefore, we measured the intrinsic Trp fluorescence of the proteins to test the acidification-dependent conformational changes (Fig. 3.5). The emission spectra of WT MtbESAT-6 showed

that there was a left shift of the peak maximum from pH 7.0 to pH 5.0 (Fig. 3.5A), suggesting a significant conformational change occurred upon acidification. In contrast, P1, P2 and P3 showed significant higher shift in the emission spectra between pH 7.0 and pH 5.0 (Fig. 3.5 B,C and D). These data are consistent with the results obtained from the ANTS/DPX dequenching assay (Fig. 3.2), and CD (Fig. 3.3). It demonstrated that acidification induced a stronger conformational change on P1, P2 and P3 compare with WT MtbESAT-6 [22].

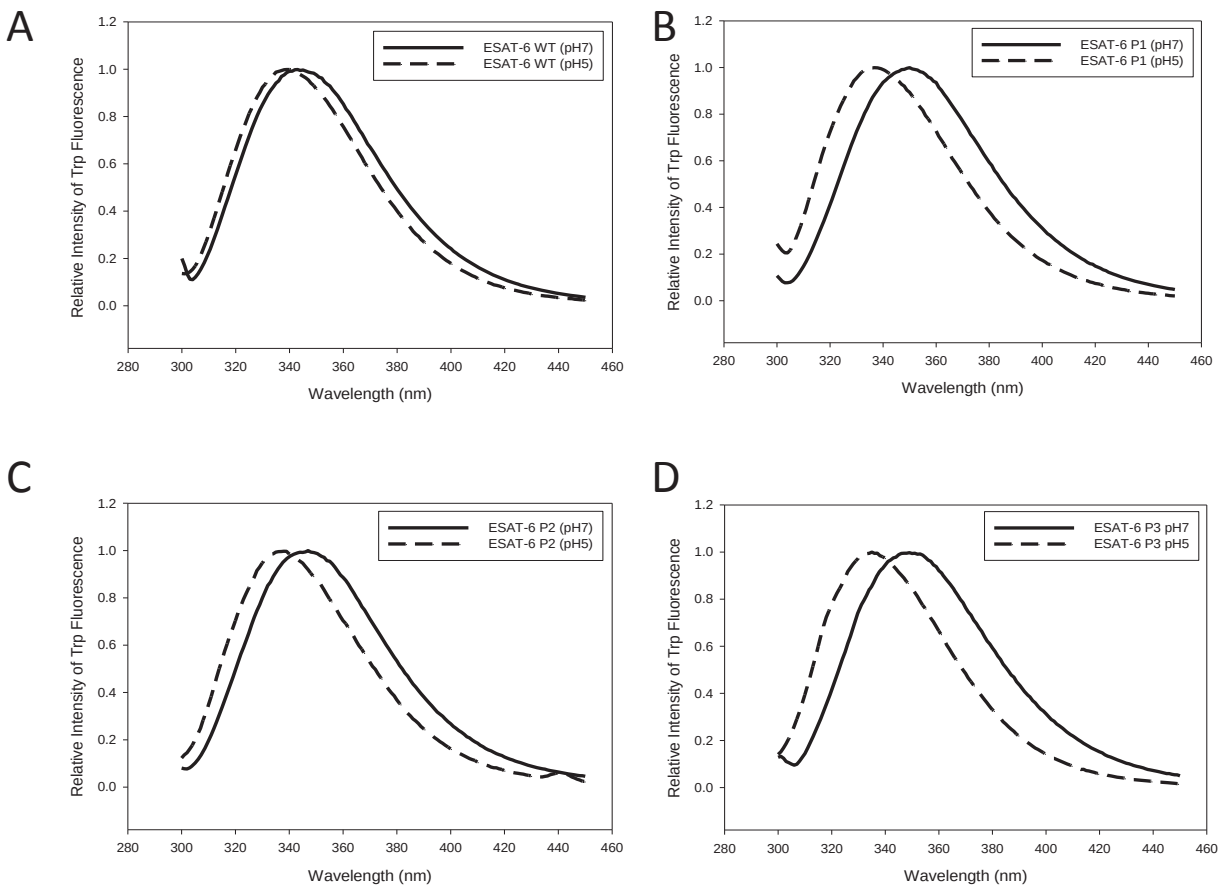

Figure 3.5 Acidification triggered a stronger conformational change on P1, P2 and P3 than WT MtbESAT-6. 10 μM of MtbESAT-6 WT (**A**), P1 (**B**), P2 (**C**) or P3 (**D**) were incubated either at pH 7.0 or at pH 5.0 for 30 min. The samples were excited at 295 nm and the emission spectra of Trp fluorescence of the samples were recorded at 310–450 nm. The emission spectra of the samples were calibrated with the emission spectra of the same buffers (pH 7.0 or pH 5.0) without proteins. The representative data from at least three independent experiments are shown in the figure.

3.8 NBD-LABELED G45C AND G60C SHOWED STRONG FLUORESCENCE SIGNAL AT LOW PH, INDICATING THAT THESE TWO AMINO ACIDS WERE UNDER HYDROPHOBIC ENVIRONMENT AFTER CONFORMATIONAL CHANGE INDUCED BY ACIDIFICATION.

To demonstrate the insertion of WT MtbESAT-6 into liposomal membranes directly, we attached an environment-sensitive dye (NBD) to introduced Cys at position of Q4C, G10C, Q34C, T37C, G45C, Q55C, A60C, and G88C and monitored their fluorescence emission intensity during membrane disruption. The intensity of NBD fluorescence at 544 nm increased upon a shift from a polar to a non-polar environment and this increase was observed from G45C and A60C (Fig.3.6) [28].

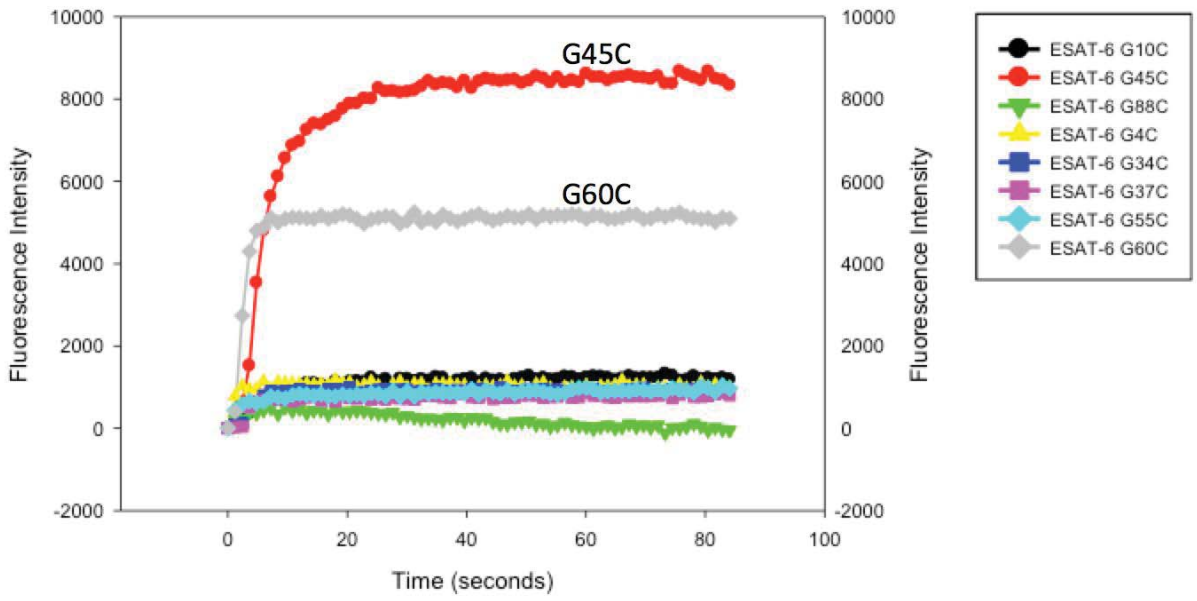

Figure 3.6 G45C and A60C showed strong fluorescence signal at low pH, indicating that those two amino acids were under hydrophobic environment after conformational change induced by acidification.

3.9 PEGS FACILITATED MTBESAT-6 MEMBRANE ACTIVITY.

It has been reported that PEGs were used to measure the size of pores on the membranes. Our previous results strongly suggested that MtbESAT-6 disrupted membrane vesicles by pore formation [29]. In this study, we chose a set of PEGs with molecular weights ranging from 600 to 10000 to measure the size of MtbESAT-6 pore, assuming that only the PEG with a similar size to the pore will partition into the ESAT-6 pore and block it (Fig. 3.7). Instead of blocking the pore, however, the result showed that PEGs significantly increased the signals of fluorescence dequenching in a size- and concentration-dependent manner. The higher molecular weight and concentration of PEGs, the better fluorescence dequenching. It suggests that PEGs assist MtbESAT-6 membrane activity with an unknown mechanism.

A

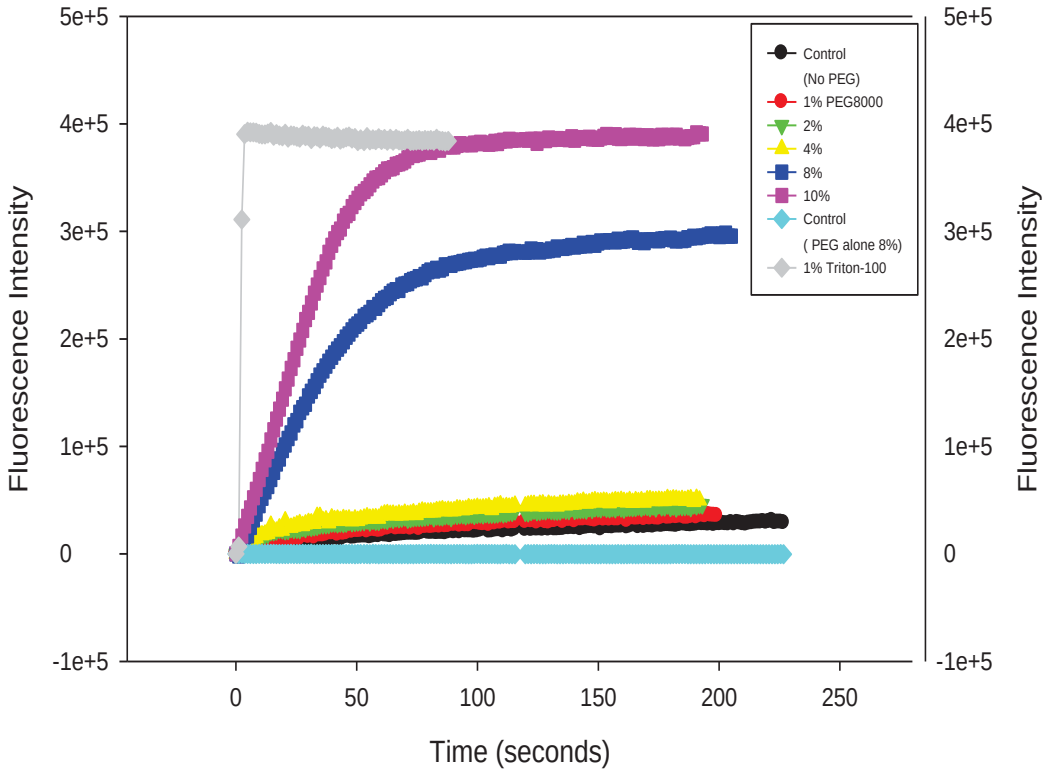
5e+5
4e+5
3e+5
2e+5
1e+5
0
-1e+5
Fluorescence Intensity
0
50
100
150
200
250
Time (seconds)
Control
(No PEG)
1% PEG8000
2%
4%
8%
10%
Control
(PEG alone 8%)
1% Triton-100

B

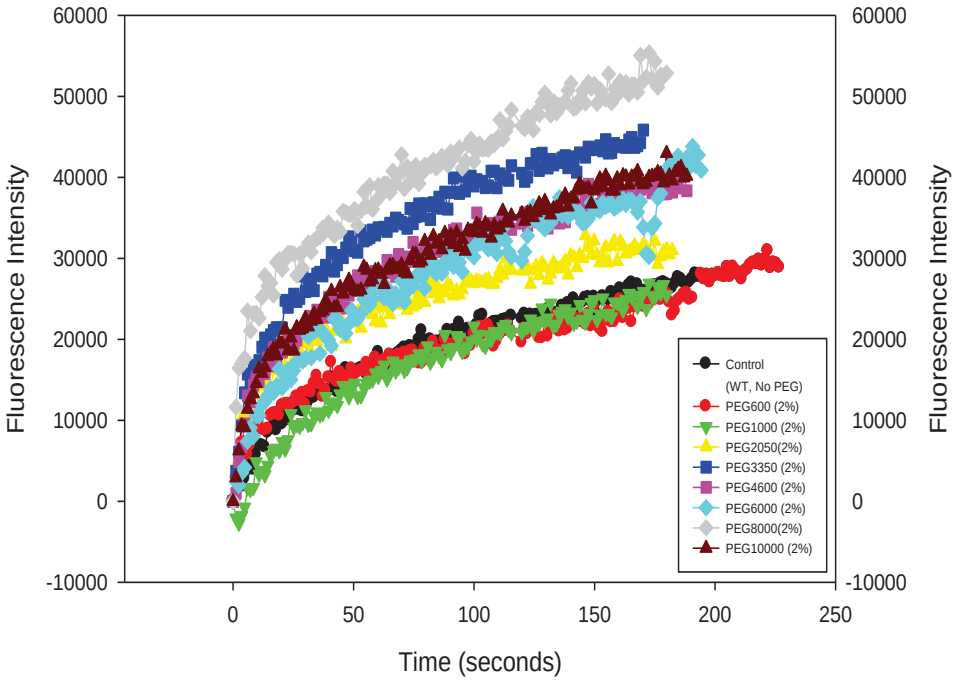

Figure 3.7 PEGs facilitated MtbESAT-6 membrane activity. Higher molecular weight and concentration of PEGs showed higher fluorescence signal, suggested that the ability of PEGs to assist MtbESAT-6 membrane activity depends on the molecular weight and concentration. The protocol followed the previously described ANTS/DPX dequenching assay except one more step was added: 5 mM of PEGs were added separately into the gel filtration butter that contains 100 µg of WT MtbESAT-6 protein and 100 µl of liposomes and incubated for 30 min. **A**. Concentration titration of PEG8000. **B**. Membrane interacting-activity facilitation by different PEGs.

CHAPTER 4: DISCUSSION

My collaboration with Joaquin De Leon identified a differential membrane interaction between MtbESAT-6 and MsESAT-6. It was confirmed that the biological functions MtbESAT-6 involved in the virulence of Mtb, which is not present in MsESAT-6. Based on this significant finding, my study further investigated the mechanism underlying the MtbESAT-6-induced virulence [22].

Using an on-column refolding approach, we purified a sufficient amount of ESAT-6 protein. This approach has proved efficient for purifying insoluble proteins. However it is not efficient for N- terminal truncations and mutants of ESAT-6 due to complications in expression in *E. coli* inclusion bodies. The alternative approach was to generate soluble ESAT-6 by GST tagging. This approach has been used with success for most of our proteins containing N-terminal truncations or mutations [30, 31].

It has been reported that C-terminus of ESAT-6 is responsible for the membrane interaction [32]. We wanted to understand the roles of N- and C- termini of ESAT-6 in membrane disruption. ANTS/DPX assay verified the importance of both N- and C-terminal flexible tails on membrane interaction activity. Deletion of either of the N- or C-terminal flexible tails resulted in a significant decrease in membrane disruption. Other experiments, such as ANS fluorescence and CD analysis, supported this result through other aspects [32, 33]. Also, relative to the rapid rate of membrane disruption caused by Triton X-100, the membrane leakage caused by MtbESAT-6 was a slower process, which suggested MtbESAT-6 formed pores on the membranes, instead of completely lysing the membranes. This phenomenon was also shown in our previous K+ release

assay [22]. Hence, we hypothesized that MtbESAT-6 caused membrane disruption by forming discrete pores on the membranes.

Combining the results from the specific aims 1 and 2, we developed a membrane insertion model of MtbESAT-6 (Fig. 4.1). According to NBD fluorescent assay, the labeling of residue Q4 showed high fluorescent even at pH 7.0 (under hydrophobic environment), suggesting that the N- terminus might be anchored onto the cell membrane before the conformational change at pH 5.0. The residues G45 and A60 showed high NBD fluorescent at pH 5.0, but not pH 7.0, suggesting that the two residues inserted into the membranes after the pH-dependent conformational change. Therefore, the hypothetical model is that N- and C- terminal flexible tails are responsible for the binding at cell surface in pH 7.0, and once the pH dropped, the two α-helixes flipped and inserted into the membranes.

ANTS/DPX fluorescent assay with PEGs was meant to measure the pore size of MtbESAT-6 based on the reported studies. Surprisingly, the PEGs showed that they facilitated pore formation of MtbESAT-6 in a dose- and molecular weight-dependent manner. A similar phenomenon was reported and inferred for the PEGs, which was due to the hydrophobic environment formed on the surface of the membrane by larger PEG molecules [34]. Future study should be focused to verify how PEGs facilitate membrane disruptions.

4.1 FUTURE DIRECTION

The further study will focus on the specific residues of both N- and C- termini of MtbESAT-6 and will identify membrane-inserting residues and their roles in membrane disruption. More hydrophobic residues should be tested in order to confirm the membrane insertion model.

Our results suggested that MtbESAT-6 disrupted the membrane by pore formation> Thus, determination of the pore size as well as the oligomeric state of ESAT-6 pore on the membrane will be a part of our work future work.

MtbESAT-6/CFP-10 might interact with other proteins during the infection, such as ClpP1 and ClpP2 [35, 36]. The truncated mutants generated in this study can be applied to the study of other binding partners of ESAT-6.

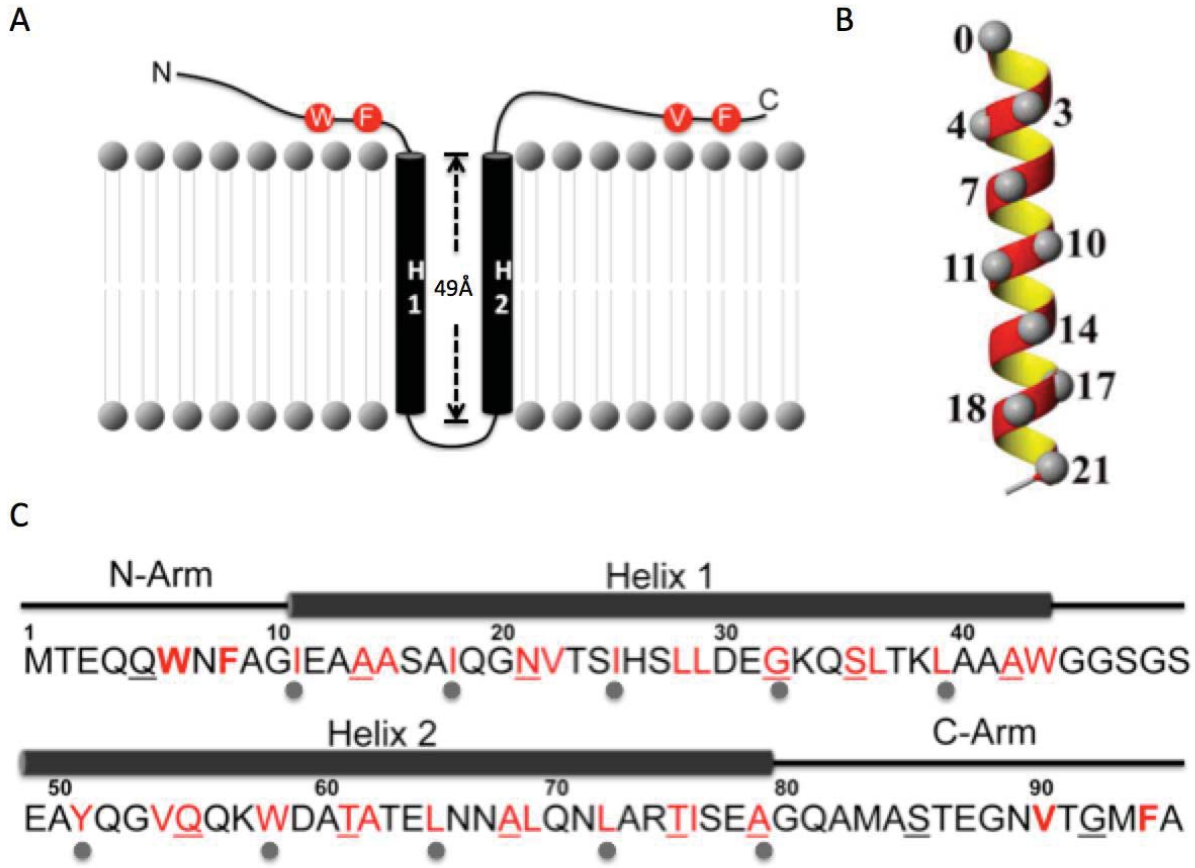

Figure 4.1: MtbESAT-6 membrane insertion model.

REFERENCES

1) Dolin, P. J., Raviglione, M. C., and Kochi, A. Global tuberculosis incidence and mortality during 1990 –2000. Bull. World Health Organ, 72: 213–220.
2) Global tuberculosis report 2012, World Health Organ.
3) David Satcher, Helene D. Gayle, Kenneth G. Castro, Stephen B. Thacker, etc. The Role of BCG Vaccine in the Prevention and Control of Tuberculosis in the United States. U.S. department of health and human services, Public health service centers for disease control and prevention (CDC).
4) Behr, M. A., Wilson, M. A., Gill, W. P., Salamon, H., Schoolnik, G. K., Rane, S., and Small, P. M. Comparative genomics of BCG vaccines by whole-genome DNA microarray. Science, 284 (1999), 1520 -1523.
5) Lewis, K. N., Liao, R., Guinn, K. M., Hickey, M. J., Smith, S., Behr, M. A., and Sherman, D. R. Deletion of RD1 from Mycobacterium tuber- culosis mimics bacille Calmette-Guérin attenuation. J. Infect. Dis, 187(2003): 117–123.
6) Guinn, K. M., Hickey, M. J., Mathur, S. K., Zakel, K. L., Grotzke, J. E., Lewinsohn, D. M., Smith, S., and Sherman, D. R. Individual RD1- region genes are required for export of ESAT-6/CFP-10 and for virulence of Mycobacterium tuberculosis. Mol. Microbiol, 51(2004): 359 –370.
7) Jessica L. Flint, Joseph C. Kowalski, Pavan K. Karnati, and Keith M. Derbyshire. The RD1 virulence locus of Mycobacterium tuberculosis regulates DNA transfer in Mycobacterium smegmatis, 101(2004): 12598–12603.
8) Krishnamohan Atmakuri and Sarah M. Fortune. Regulation of Protein Secretion by Protein Secretion? Cell Host & Microbe, 4 (2008): 190-191.

9) Jason A. MacGurn, Jeffery S. Cox. A Genetic Screen for Mycobacterium tuberculosis Mutants Defective for Phagosome Maturation Arrest Identifies Components of the ESX-1 Secretion System. Infection and immunity, 75 (2007): 2668–2678.

10) Fortune, S.M., Jaeger, A., Sarracino, D.A., Chase, M.R., Sassetti, C.M., Sherman, D. R., Bloom, B. R., and Rubin, E. J. Mutually dependent secretion of proteins required for mycobacterial virulence. Proc. Natl. Acad. Sci. U.S.A., 102 (2005): 10676 –10681.

11) Philip S Renshaw, Kirsty L Lightbody, Vaclav Veverka, Fred W Muskett, Geoff Kelly, Thomas A Frenkiel, Stephen V Gordon, R Glyn Hewinson, Bernard Burke, Jim Norman, Richard A Williamson, and Mark D Carr1. Structure and function of the complex formed by the tuberculosis virulence factors CFP-10 and ESAT-6. The EMBO Journal, 24 (2005), 2491–2498.

12) Buka Samten, Xisheng Wang, Peter F. Barnes. Mycobacterium tuberculosis ESX-1 system-secreted protein ESAT-6 but not CFP10 inhibits human T-cell immune responses. B. Tuberculosis, 89 (2009) S74–S76.

13) Laxman S. Meena and Rajni. Survival mechanisms of pathogenic Mycobacterium tuberculosis H37Rv. FEBS Journal, 277 (2010) 2416–2427.

14) van der Wel, N., Hava, D., Houben, D., Fluitsma, D., van Zon, M., Pierson, J., Brenner, M., and Peters, P. J. M. tuberculosis and M. leprae translocate from the phagolysosome to the cytosol in myeloid cells. Cell, 129 (2007): 1287–1298.

15) Simeone, R., Bobard, A., Lippmann, J., Bitter, W., Majlessi, L., Brosch, R., and Enninga, J. Phagosomal rupture by Mycobacterium tuberculosis results in toxicity

and host cell death. PLoS Pathog, 8 (2012): e1002507.

16) Eun-Kyeong Jo, Jae-MinYuk, Dong-Min Shin and Chihiro Sasakawa. Roles of autophagy in elimination of intracellular bacterial pathogens, 4 (2013): 1-9.

17) Keane Joseph, Heinz G. Remold,Hardy Kornfeld, Host Defense: Virulent Mycobacterium tuberculosis Strains Evade Apoptosis of Infected Alveolar Macrophages, J Immunol, 164 (2000):2016-2020.

18) Kang, P. B., Azad, A. K., Torrelles, J. B., Kaufman, T. M., Beharka, A., Tibesar, E., DesJardin, L. E., and Schlesinger, L. S. The human macrophage mannose receptor directs Mycobacterium tuberculosis lipoarabinomannan-mediated phagosome biogenesis. J. Exp. Med, 202 (2005): 987–999.

19) Rohde, K., Yates, R. M., Purdy, G. E. and Russell, D. G. Mycobacterium tuberculosis and the environment within the phagosome. Immunological Reviews, 219 (2007): 37–54.

20) Omar H. Vandal, Carl F. Nathan and Sabine Ehrt. Acid Resistance in Mycobacterium tuberculosis. J. Bacteriol, 191(2009) :4714- 4721.

21) Renshaw, P. S., Panagiotidou, P., Whelan, A., Gordon, S. V., Hewinson, R. G., Williamson, R. A., and Carr, M. D. Conclusive evidence that the major T-cell antigens of the Mycobacterium tuberculosis complex ESAT-6 and CFP-10 form a tight, 1:1 complex and characterization of the structural properties of ESAT-6, CFP-10, and the ESAT-6*CFP-10 com- plex. Implications for pathogenesis and virulence. J. Biol. Chem. 277 (2002), 21598 –21603.

22) Joaquin De Leon, Guozhong Jiang, Yue Ma,Eric Rubin, Sarah Fortune and Jianjun Sun. Mycobacterium tuberculosis ESAT-6 Exhibits a Unique Membrane-

interacting Activity That Is Not Found in Its Ortholog from Non-pathogenic Mycobacterium smegmatis. The journal of biological chemistry, 287 (2012): 44184-44191.

23) Sun, J., Vernier, G., Wigelsworth, D. J., and Collier, R. JInsertion of anthrax protective antigen into liposomal membranes: effects of a receptor. J. Biol. Chem. 282 (2007): 1059 –1065.

24) Sun, J., Lang, A. E., Aktories, K., and Collier, R. J. Phenylalanine-427 of anthrax protective antigen functions in both pore formation and protein translocation. Proc. Natl. Acad. Sci. U.S.A. 105 (2008), 4346 – 4351.

25) Marais BJ, Hesseling AC, Gie RP, et al. The burden of childhood tuberculosis and the accuracy of community-based surveillance data. Int J Tuberc Lung Dis, 10 (2006): 259–263.

26) Marien I. de Jonge, Ge´rard Pehau-Arnaudet, Marjan M. Fretz, Felix Romain, Daria Bottai, Priscille Brodin, Nadine Honore, Gilles Marchal, Wim Jiskoot, Patrick England, Stewart T. Cole, Roland Brosch. ESAT-6 from Mycobacterium tuberculosis Dissociates from Its Putative Chaperone CFP-10 under Acidic Conditions and Exhibits Membrane-Lysing Activity. Journal of Bacteriology, 189 (2007): 6028-6034.

27) Venyaminov, S.Y., and Yang, J.T. Determination of protein secondary structure, in Circular Dichroism and the Conformational Analysis of Biomolecules. Plenum Press. (1996): 69–107.

28) Kirsty L. Lightbody, Dariush Ilghari, Lorna C. Waters, Gemma Carey, Mark A. Bailey, Richard A. Williamson, Philip S. Renshaw, and Mark D. Carr. Molecular

Features Governing the Stability and Specificity of Functional Complex Formation by Mycobacterium tuberculosis CFP-10/ESAT-6 Family Proteins. The journal of biological chemistry, 283 (2008): 17681-17690.

29) Jennifer Smith, Joanna Manoranjan,Miao Pan, Amro Bohsali,1 Junjie Xu, Jun Liu, Kent L. McDonald, Agnieszka Szyk, Nicole LaRonde-LeBlanc, and Lian-Yong Gao. Evidence for Pore Formation in Host Cell Membranes by ESX-1-Secreted ESAT-6 and Its Role in Mycobacterium marinum Escape from the Vacuole. Infection and Immunity, 76 (2008): 5478-5487.

30) Renshaw, P. S., Lightbody, K. L., Veverka, V., Muskett, F. W., Kelly, G., Frenkiel, T. A., Gordon, S. V., Hewinson, R. G., Burke, B., Norman, J., Williamson, R. A., and Carr, M. D. Structure and function of the complex formed by the tuberculosis virulence factors CFP-10 and ESAT-6. EMBO J, 24 (2005): 2491–2498.

31) Lightbody, K. L., Ilghari, D., Waters, L. C., Carey, G., Bailey, M. A., Wil- liamson, R. A., Renshaw, P. S., and Carr, M. D. Molecular features governing the stability and specificity of functional complex formation by Mycobacterium tuberculosis CFP-10/ESAT-6 family proteins. J. Biol. Chem, 283 (2008): 17681–17690.

32) Brodin, P., de Jonge, M. I., Majlessi, L., Leclerc, C., Nilges, M., Cole, S. T., and Brosch, R. Functional analysis of early secreted antigenic target-6, the dominant T-cell antigen of Mycobacterium tuberculosis, reveals key residues involved in secretion, complex formation, virulence, and immunogenicity. J Biol Chem, 280(2005): 33953–33959.

33) Woody, R.W., and Dunker, A.K. Aromatic and cystine side-chain circular dichroism in proteins, in Circular Dichroism and the Conformational Analysis of

Biomolecules. Plenum Press, (1996): 109–157.

34) Danying Zuo, Youyi Xu, Weilin Xu and Hantao Zou. The influence of PEG molecular weight on morphologies and propertites of PVDF asymmetric membranes. Chinese Journal of Polymer Science. 26 (2008): 405-414.

35) Raju, R. M., Unnikrishnan, M., Rubin, D. H., Krishnamoorthy, V., Kan- dror, O., Akopian, T. N., Goldberg, A. L., and Rubin, E. J. Mycobac- terium tuberculosis ClpP1 and ClpP2 function together in protein degra- dation and are required for viability in vitro and during infection. PLoS Pathog, 8(2012), e1002511.

36) Akopian, T., Kandror, O., Raju, R. M., Unnikrishnan, M., Rubin, E. J., and Goldberg, A. L. The active ClpP protease from M. tuberculosis is a complex composed of a heptameric ClpP1 and a ClpP2 ring. EMBO J, 31(2012): 1529 - 1541.

CURRICULUM VITA

Yue Ma was born in Qiqihar, Heilongjiang in China. She grew up there and lived there until she graduated from high school. She then attended Harbin Medical University with a Bachelor of Science in Pharmacy. After finishing with her undergraduate work, she went on to complete her Master of Science in Pharmaceutical at Zhengzhou University. Upon graduation, she worked in Salubris Pharmaceutical Company before deciding to study biological sciences in the United States at the University of Texas at El Paso. She worked as a teaching assistant and taught General Biology laboratory and Anatomy to undergraduate students at the university. Aside from science, she enjoys writing, traveling and cooking. Her long-term goals are to understand life from different perspectives and opinions.

Address: 2401 North Oregon

El Paso, El Paso 79902

This thesis was typed by Yue Ma.